Research Square

Preprints are preliminary reports that have not undergone peer review.
They should not be considered conclusive, used to inform clinical practice,
or referenced by the media as validated information.

Bioprospecting Fermented Millet-Derived Limosilactobacillus fermentum for In Vitro Antiplasmodial Activity, Biochemical Profiling, and In Silico Characterization of Geranyl Pyrophosphate and Novel Bioactive Peptides

Caroline Amuche Okoli

caroalph@yahoo.com

University of Jos https://orcid.org/0009-0005-0745-1060

Norah Ashezi Ephraim

University of Jos

Tok Simi Sunday

University of Jos

Blessing Nnawo Lile

University of Jos

Research Article

Keywords: Aminopeptidase triad, Antiplasmodial peptides, Bioprospecting, Fermented millet, Geranyl pyrophosphate, Limosilactobacillus fermentum, Molecular docking, Plasmodium falciparum, Probiotics

Posted Date: October 6th, 2026

DOI: https://doi.org/10.21203/rs.3.rs-11252319/v1

License: This work is licensed under a Creative Commons Attribution 4.0 International License.
Read Full License

Additional Declarations: The authors declare no competing interests.

Bioprospecting Fermented Millet-Derived Limosilactobacillus fermentum for In Vitro Antiplasmodial Activity, Biochemical Profiling, and In Silico Characterization of Geranyl Pyrophosphate and Novel Bioactive Peptides

[*1,2,3]Caroline Amuche Okoli, [1]Norah Ashezi Ephraim, [1]Tok Simi Sunday, [1]Blessing Nnawo Lile

1. Chemical Pat hology Unit, Department of Medical Laboratory Science, Faculty of Health Sciences and Technology, College of Health Sciences, University of Jos, Jos, Nigeria
2. Department of Biochemistry, Faculty of Basic Medical Sciences, College of Health Sciences University of Jos, Nigeria
3. Initiatives for Accessible Genomics and Bioinformatics, Genomic House, Little Rayfield, Jos, Nigeria

***Correspondence**

Caroline Amuche Okoli (PhD)
Chemical Pathology Unit,
Department of Medical Laboratory Science
University of Jos, Jos,
Nigeria.
okolic@unijos.edu.ng
caroalph@yahoo.com
+234-9038864706

Background

The rising global threat of drug-resistant *Plasmodium falciparum* demands novel, multi-targeted antimalarial therapeutics. Probiotic lactic acid bacteria, notably *Limosilactobacillus fermentum* from traditional fermented cereal matrices, offer a promising source of functional metabolites and bioactive secretome peptides.

Methods

This study integrated *in vitro*, bioinformatic, and chemoinformatic pipelines to evaluate biogenic geranyl pyrophosphate (GPP) and novel secretome peptides (IITAAFGQFLPDKLLAAAKV, LILKLVKTPDILKTMGQKKG, and GASRASFPTILASGPNSAKP) from *L. fermentum* isolated from laboratory-fermented millet broth and commercial *kunu-zaki*. *In vitro* antiplasmodial efficacy and host erythrocyte hemolysis were evaluated using clinical parasite isolates from ten malaria-positive patients at Plateau State Specialist Hospital, Jos, Nigeria. Intracellular lysate (ICL) and cell-free supernatant (CFS) fractions were assayed for lactic acid and protein yields. Whole-genome sequences were mined using antiSMASH 7.0 and NCBI BLAST. Peptide potential, tertiary structures, multi-target docking against *P. falciparum* aminopeptidases (PDB: 5YIQ, 5YIH, 5Y3I), and safety profiles were evaluated using CAMPr3, APD3, PEP-FOLD3, HDOCK, AutoDock Vina, ProTox-3.0, ToxinPred, AllerTOP v2.0, and HemoPI.

Results

Limosilactobacillus fermentum isolates demonstrated strong antiplasmodial activity with 0% host erythrocyte hemolysis. High concentrations of lactic acid and proteins were recovered from CFS and ICL. Genomic analysis confirmed novel biosynthetic gene clusters, while machine learning models predicted high antimicrobial efficacy. Peptides formed stable tertiary structures with high binding affinity across target aminopeptidases ($\Delta G = -7.6$ kcal/mol), stabilized by hydrogen bonds, salt bridges, and hydrophobic contacts. *In silico* profiles confirmed GPP was non-hepatotoxic, non-nephrotoxic, non-cardiotoxic, and non-mutagenic (BBB= 1.00), while candidate peptides were non-toxic, non-allergenic, and non-hemolytic (HemoPI ≤ 0.00).

Conclusion

Biogenic GPP and novel *L. fermentum* peptides display favorable therapeutic indices, multi-target binding, and safe pharmacokinetic profiles, representing promising leads for antimalarial drug development.

.

Key words: Aminopeptidase triad, Antiplasmodial peptides, Bioprospecting, Fermented millet, Geranyl pyrophosphate, *Limosilactobacillus fermentum*, Molecular docking, *Plasmodium falciparum*, Probiotics.

Introduction

Malaria remains a major global public health threat in tropical and subtropical regions. Globally in 2024, there were an estimated 282 million malaria cases and 610,000 deaths across 80 endemic countries, with the African Region bearing the highest burden [1, 2]. Nigeria accounts for the largest share of the global malaria burden, contributing an estimated 68 million cases and 184,800 deaths in 2025 [1]. Beyond its devastating clinical toll, malaria imposes substantial economic burdens on individuals, national health systems, and international development [2, 3].

Human malaria is caused by five protozoan species of the genus *Plasmodium*, among which *Plasmodium falciparum* is the most virulent and prevalent on the African continent [4]. The primary mode of transmission is the bite of an infected female *Anopheles* mosquito, although secondary transmission occurs via blood transfusion, organ transplantation, contaminated needle sharing, and congenital transfer [4, 5]. The parasite lifecycle spans the sporogonic phase in the mosquito vector, followed by exoerythrocytic (hepatic) and erythrocytic developmental stages in the human host [4–6].

Vector control measures—including insecticide-treated nets (ITNs) and indoor residual spraying (IRS)—alongside antimalarial chemotherapeutics have significantly reduced disease incidence over recent decades [1, 7]. However, *P. falciparum* has successfully evolved resistance to every class of antimalarial drug introduced into clinical practice [7]. Contemporary therapeutic strategies rely on artemisinin-based combination therapies (ACTs) as frontline treatment [7, 8]. While frontline ACTs maintain efficacy in Nigeria and broader West Africa, the clonal expansion of

validated *P. falciparum* kelch13 (*pfk13*) propeller mutations—such as R561H in Rwanda [9, 10] and A675V/C469Y in Uganda [11, 12]—highlights the growing threat of partial artemisinin resistance across Sub-Saharan Africa [7, 13]. Although genomic surveillance indicates that validated *pfk13* mutations remain below 2% in Nigeria [14, 15], high background fixation of *pfcrt* K76T chloroquine-resistance markers (50%–85%) [16] and *pfdhfr*/*pfdhps* antifolate-resistance alleles [17, 18] underscores the urgent need for novel, non-cross-resistant therapeutic leads [19].

Addressing antimalarial resistance requires integrating host-pathogen immunology with novel bioprospecting paradigms. Pathogenesis is driven by parasite products that stimulate proinflammatory and counter-regulatory cytokine responses across innate and adaptive immune cells [20–22]. This immunological cross-talk opens avenues for utilizing commensal microorganisms or probiotics to modulate host immune responses [23, 24]. Evidence indicates that gut microbiota composition influences malaria severity in animal models [25–27] and clinical settings [28–30]. Lactic acid bacteria (LAB), particularly *Lactobacillus* and *Limosilactobacillus* species, produce antimicrobial peptides (bacteriocins), organic acids (lactic and acetic acid), and secondary metabolites (terpenes, isoprenoids) that inhibit pathogenic organisms [31, 32]. Furthermore, systemic probiotic effects influence the gut-brain axis, potentially mitigating neurological complications associated with severe cerebral malaria [33–35].

Consequently, there is an imperative to develop next-generation antimalarials possessing high genetic barriers to resistance, simple dosing regimens, rapid parasiticidal clearance, and excellent host safety profiles [19, 36]. Bioprospecting *Limosilactobacillus fermentum* from traditional

fermented food matrices offers a sustainable strategy to harvest bioactive small molecules and functional peptides [37]. Probiotic LAB from traditional fermented cereal foods—such as *L. fermentum* isolated from "Kunu-zaki" (a traditional Nigerian fermented cereal beverage) or fermented millet—produce secretome peptides with intrinsic antiparasitic properties [38, 39]. Pearl millet (*Pennisetum glaucum*) is a climate-resilient, drought-tolerant grain well-adapted to arid and semi-arid environments, making it vital for food security and sustainable agriculture in Sub-Saharan Africa [40, 41]. Spontaneous or controlled fermentation of millet utilizes microbial metabolism to enhance nutritional value, extend shelf life, and generate functional organic acids, bioactive peptides, and secondary metabolites [42–44].

Unlike broad plant extracts or synthetic small molecules, bioactive peptides offer high target specificity, favorable safety profiles, non-toxic metabolic degradation products, lower immunogenicity, lack of host hemolysis, and suitability for rational *in silico* optimization [45, 46]. Among secondary metabolites, monoterpene intermediates like geranyl pyrophosphate (GPP) play vital roles in isoprenoid biosynthesis [47], whereas ribosomally synthesized and post-translationally modified peptides (RiPPs) or secretome-derived peptide fragments provide targeted receptor-binding capabilities [48].

Historically, isolating and characterizing antiplasmodial candidate sequences from raw bacterial secretomes required high-cost, labor-intensive screening. To overcome these limitations, machine learning algorithms—such as CAMPr3 (utilizing Support Vector Machine, Random Forest, Artificial Neural Network and Discriminant Analysis architectures) [49] and APD3 (Antimicrobial

Peptide Database) [50]—can rapidly screen proteomic sequences *in silico*. Subsequent 3D structural modeling via PEP-FOLD3 [51] and multi-target molecular docking against essential *P. falciparum* receptors provide a rational design roadmap prior to solid-phase synthesis and empirical validation.

In this study, we targeted three essential *P. falciparum* neutral aminopeptidases which include,

PfA-M1 (PDB: 5YIQ)- A zinc-dependent M1 family alanyl aminopeptidase that cleaves neutral and hydrophobic N-terminal amino acids from oligopeptides during hemoglobin degradation in the digestive vacuole and cytosol, providing free amino acids essential for parasite protein synthesis, osmoregulation, and survival [52, 53]. **PfM18AAP (PDB: 5YIH)-** An M18 family aspartyl aminopeptidase responsible for cleaving acidic N-terminal residues from hemoglobin-derived peptides, operating synergistically with PfA-M1 and PfA-M17 [54]. **PfA-M17 (PDB: 5Y3I)-**A zinc-dependent M17 leucyl aminopeptidase that cleaves N-terminal hydrophobic residues during the final stages of cytosolic oligopeptide proteolysis [55].

Together, this aminopeptidase triad (PfA-M1, PfM18AAP, and PfA-M17) functions across erythrocytic, liver, and sexual (gametocyte) stages of *P. falciparum*, offering pan-stage therapeutic utility [52–55]. Although human orthologs exist (e.g., human CD13/alanyl aminopeptidase and leucyl aminopeptidase), structural differences in the parasite catalytic binding pockets allow synthetic and natural inhibitors to achieve high pathogen specificity without cross-inhibiting human enzymes, minimizing host cytotoxicity [52, 56].

We formulated two testable hypotheses. Firstly, hypothesis A (Metabolite–Protein Interaction) which states that Biogenic GPP derived from *L. fermentum* acts as a competitive metabolic inhibitor that binds directly to essential *P. falciparum* aminopeptidases and disrupts apicoplast isoprenoid biosynthesis via the non-mevalonate 1-deoxy-D-xylulose 5-phosphate (DOXP) pathway [47, 57]. Secondly, hypothesis B (Peptide–Protein Macromolecular Interaction) which postulates that Secretome-derived short peptides (IITAAFGQFLPDKLLAAAKV, LILKLVKTPDILKTMGQKKG, and GASRASFPTILASGPNSAKP) bind with high affinity to the active-site geometry of the PfA-M1, PfM18AAP, and PfA-M17 catalytic triad, competitively inhibiting hemoglobin digestion and osmotic regulation [52–55].

Here, we present an integrated experimental, computational, bioinformatic, and toxicological evaluation of biogenic GPP and three novel bioactive peptides harvested from *L. fermentum*. We systematically assessed their *in vitro* antiplasmodial efficacy, structural docking dynamics, and pharmacokinetic safety profiles to evaluate their potential as antimalarial lead candidates.

Materials and Methods

Study Design and Study Area

This study employed an integrated *in vitro* experimental and *in silico* computational design. Laboratory procedures were carried out in the Research Laboratory of the Department of Medical Laboratory Science, Faculty of Health Sciences and Technology, University of Jos, Plateau State, Nigeria.

Study Population and Ethical Considerations

The study population comprised ten (n = 10) clinical malaria-infected patients and one (n = 1) non-infected (malaria-negative) control individual attending the outpatient clinics at Plateau State Specialist Hospital, Jos, Plateau State, Nigeria. Diagnostic confirmation of *Plasmodium falciparum* infection was established microscopically.

Preparation and Fermentation of Substrates and Sample Sourcing

Two separate matrices were utilized for the isolation of probiotic *Limosilactobacillus fermentum*: a controlled laboratory-fermented millet slurry and a commercial fermented cereal beverage ("Kunu-zaki").

1. **Laboratory Fermented Millet Slurry:** Prepared using a modification of the protocol described by Zakariya et al. [58]. Pearl millet (*Pennisetum glaucum*) grains were thoroughly washed in sterile distilled water and soaked in sterile distilled water within sterile universal containers at room temperature (25^{o}C for 24 hours. The soaked grains were

rinsed, homogenized using a pre-sterilized laboratory blender, and strained through sterile muslin cloth. The resulting slurry was transferred into sterile universal bottles and allowed to undergo natural anaerobic fermentation at room temperature (25^{o}C) for an additional 24 hours.

2. **Commercial "Kunu-zaki":** Fresh, ready-to-consume "Kunu-zaki" samples (composed of fermented millet, ginger, cloves, malted rice seedlings, and sweet potato) were obtained from a commercial vendor in Jos, Nigeria, transported under refrigerated conditions (4^{o}C), and processed within 2 hours of collection.

Culture, Isolation, and Phenotypic Identification of *Limosilactobacillus fermentum*

Substrates from fermented millet slurry and "Kunu-zaki" were cultured onto De Man, Rogosa, and Sharpe (MRS) agar (ReadyMED, Chaitanya Agro Bio-Tech Pvt. Ltd., India) for the selective isolation of lactic acid bacteria [59,60]. MRS agar (67.50 g/L) was dissolved in sterile distilled water, autoclaved at 121^{o}C, 15 psi for 15 minutes, cooled to 45^{o}C and aseptically poured into sterile Petri dishes. Tenfold serial dilutions of the fermented matrices (1×10^{6} to 10×10^{6} colony forming unit (CFU) were inoculated onto the dried MRS plates via the spread-plate method [60]. Culturing was made in duplicate plates. Plates were incubated microaerophilicly at 2 different temperatures of 15^{o}C and 45^{o}C for 24hours. Distinct single colonies were picked and subcultured iteratively onto fresh MRS agar to obtain pure isolate cultures.

Phenotypic characterization and physiological identification of *L. fermentum* were conducted according to established taxonomic criteria [59]. Isolates were identified based on colonial

morphology, Gram staining, motility, endospore formation, catalase testing, temperature tolerance 15ºC versus 45ºC, citrate utilization, urease activity, and carbohydrate fermentation patterns on Kligler Iron Agar (KIA).

Presumptive *L. fermentum* isolates were confirmed based on the following phenotypic profile:

- Opaque, smooth, creamy, circular convex colonies (1-3 mm in diameter) on MRS agar;
- Gram-positive, non-motile, non-spore-forming bacilli;
- Catalase-negative and urease-negative reactions;
- Growth at 15ºC with no growth at 45ºC
- Negative for citrate utilization;
- KIA profile demonstrating acid slant (slant), acid butt , with absence of hydrogen sulfide production and gas formation.

Diagnostic Malaria Microscopy and Parasite Quantification

Venous blood 2 ml was drawn from each participant via venipuncture into ethylenediaminetetraacetic acid (EDTA) vacuum tubes under aseptic conditions. Thick and thin blood films were prepared on clean glass slides, fixed (thin films only, with absolute methanol), and stained with freshly prepared 30% Giemsa solution pH 7.2 for 10 minutes [61-62]. Parasite species identification was performed on thin films under oil immersion lens (x100 magnification). Parasite density was quantified on thick films by counting asexual *P. falciparum* stages against

200 white blood cells (WBCs) and calculated assuming a standard leukocyte count of 8,000 WBCs/µl [61-62].

Parasite Density ($x10^3$ parasites/µl = $\frac{Asexual\ Parasites\ Counted)\ x\ 8{,}000\ WBCs}{\{200)\ WBCs}$

Short-Term *In Vitro* Culture of *Plasmodium falciparum*

Culture media was formulated using McCoy's 5A modified medium (Merck, Germany). Briefly, 25g of powder was reconstituted in 40 mL of double-distilled water, supplemented with sodium bicarbonate and adjusted to pH 7.2 -7.4. The total volume was made up to 200 ml and filter-sterilized using a 0.22µm polyethersulfone (PES) membrane vacuum filtration unit [63]. Parasites were maintained short-term in McCoy's 5A medium supplemented with 10% ABO-compatible human serum at a baseline hematocrit of 5%

***In Vitro* Antiplasmodial Screening and Red Blood Cell Hemolysis Assays**

Preparation of *L. fermentum* Bacterial Working Suspensions

Single discrete colonies of confirmed *L. fermentum* were inoculated into sterile peptone water and incubated at 37ºC for 30 minutes to adjust turbidity to a 0.5 McFarland standard (approx. 1×10^8 CFU/mL}. Serial dilutions were performed in sterile phosphate-buffered saline (PBS, pH} 7.4) to yield standardized working bacterial suspensions ranging from 1×10^6 to 10×10^6 CFU/mL}[64].

Experimental Co-Incubation Assays

Antiplasmodial testing was performed in sterile multi-well microplates following modified short-term susceptibility protocols [64, 65]. Aliquots (200 µl} of prepared McCoy's 5A culture medium were transferred into designated wells, followed by the addition of 20µl of *P. falciparum*-infected human erythrocytes (2-5% baseline parasitemia). Standardized *L. fermentum* suspensions 1 $x10^6$ to 10 x 10^6 CFU/mL were added to experimental wells. Plates were incubated microaerophilically (5% CO_2, 5% O_2, 90% N_2) at 37°C for 2 hours and 4 hours to evaluate parasite clearance kinetics.

Experimental design controls included:

1. **Negative Parasite Control:** Parasitized erythrocytes in McCoy's 5A culture medium without bacterial or drug exposure [65];
2. **Positive Drug Control:** Parasitized erythrocytes treated with chloroquine diphosphate at 320ng/mL} (standard threshold derived from WHO Mark III susceptibility assay criteria) [65];
3. **Uninfected Red Blood Cell Safety Control:** Non-infected donor erythrocytes (20µl co-incubated directly with live *L. fermentum* suspensions ($10x10^6$ CFU/ml to evaluate bacterial-induced direct erythrocyte hemolysis or membrane deformation [66].

Following exposure, thick blood smears were prepared in duplicate, stained with 30% freshly prepared Giemsa, and evaluated under oil immersion (x 100) to determine post-exposure parasitemia and parasite clearance rates [61-62].].

Biochemical Characterization of Active Subcellular Fractions

To evaluate the biochemical basis of the antiplasmodial effect, *L. fermentum* cultures were separated into intracellular lysates (ICL) and cell-free extracellular supernatants (CFS) [67].

A 5ml aliquot of logarithmic-phase live bacterial culture was centrifuged at 4,000 x g for 15 minutes at 4ºC. The decanted supernatant was filtered through a 0.22µm membrane filter to obtain the cell-free extracellular supernatant (CFS). The remaining cell pellet was washed three times in ice-cold PBS (pH 7.4) by centrifugation at 4,000g for 10 minutes. Washed cells were resuspended in PBS and subjected to thermal lysis in a boiling water bath (100ºC) for 15 minutes to release intracellular contents, followed by centrifugation at 10,000 g for 10 minutes to clear cellular debris, yielding the intracellular lysate (ICL) [67].

Determination of Lactic Acid Concentrations

Titratable acidity in ICL and CFS fractions was quantified via acid-base neutralization titrations [68]. Aliquots (10ml) of each fraction were titrated against standardized (0.1 M NaOH) using 1% phenolphthalein as an indicator. Standardized 0.1 M HCl was titrated concurrently to calibrate calculations. Total lactic acid percentage was determined using the formula:

$$Lactic\ Acid\ (\%\ w/v)\ =\ Volume\ of\ NaOH\ x\ normality\ of\ NaOH\}\}\ x\ 90.08$$

$$Volume\ of\ sample\ x\ 10$$

90.08 is the equivalent molecular weight of lactic acid g/mol

Determination of Total Protein Content

Protein concentrations in ICL and CFS were quantified using trichloroacetic acid (TCA) precipitation followed by Biuret colorimetric determination. Proteins were precipitated from 1 ml sample aliquots using an equal volume of cold 100%(w/v) TCA and centrifuged at 8,000 for 10 minutes. Protein pellets were washed thrice with ice-cold acetone to remove residual acid, dissolved in 0.1M NaOH and reacted with Biuret reagent under alkaline conditions. Absorbance was recorded at 540nm using a UV-Vis spectrophotometer. Bovine Serum Albumin (BSA, 10mg/ml) served as the quantification standard.

Statistical Analysis

Data were analyzed using IBM SPSS Statistics for Windows, Version 27.0 (IBM Corp., Armonk, NY, USA). Continuous variables (lactic acid and protein yields) were expressed as Mean± Standard Deviation (SD). Differences between experimental and control groups were evaluated using one-way Analysis of Variance (ANOVA) followed by Tukey's *post-hoc* tests. Statistical significance was set at $p \leq 0.05$

***In Silico* Computational Mining and Structural Characterization**

Whole-Genome Retrieval and Secondary Metabolite Gene Cluster Analysis

Genomic Sequence Read Archive (SRA) and whole-genome assembly datasets corresponding to twelve (n = 12) *Limosilactobacillus fermentum* strains were retrieved from the National Center for Biotechnology Information (NCBI) database. Secondary metabolite Biosynthetic Gene Clusters (BGCs) were identified and annotated using the Antibiotics and Secondary Metabolites Analysis Shell (antiSMASH v7.0) framework [69]. Sequence novelty was established by subjecting predicted candidate clusters and precursor proteomic sequences to search algorithms via NCBI Basic Local Alignment Search Tool (BLASTp and BLASTn) against non-redundant nucleotide and protein databases.

Machine Learning Antimicrobial and Antiplasmodial Screening

Candidate peptide sequences derived from *L. fermentum* precursor proteomes were submitted to machine learning classifiers integrated within the Collection of Anti-Microbial Peptides (CAMPr3) database [49] and the Antimicrobial Peptide Database (APD3) [50]. Sequence propensity was evaluated using four distinct algorithmic models:

- Support Vector Machine (SVM);
- Random Forest (RF);
- Artificial Neural Network (ANN);
- Discriminant Analysis (DA).

Physicochemical parameters—including net charge, hydrophobicity index, hydrophobic moment, and isoelectric point (pI)—were calculated using the ExPASy ProtParam tool. Initial algorithmic screening yielded six high-probability antimicrobial peptides:

1. IITAAFGQFLPDKLLAAAKV (AMP-1)
2. LILKLVKTPDILKTMGQKKG (AMP-2)
3. WPKLSKAAVAKRLVALIGQR (AMP-3)
4. GASRASFPTILASGPNSAKP (AMP-4)
5. LKQACYGATAGIQLARGFVA (AMP-5)
6. ILDRKGK (AMP-6)

Following preliminary structural modeling, candidate peptides AMP-5 (LKQACYGATAGIQLARGFVA) and AMP-6 (ILDRKGK) were excluded from downstream analyses due to unfavorable target binding energies ($\Delta G > -5.0$ kcal/mol). The remaining candidates (AMP-1, AMP-2, AMP-3, and AMP-4) were confirmed to be novel short peptides without exact sequence hits in public databases.

Target Selection and Structure Preparation

Three essential *P. falciparum* neutral aminopeptidases were selected as macromolecular receptors based on their coordinated catalytic role in erythrocytic and liver-stage hemoglobin proteolysis:

1. **PfA-M1 (PDB ID: 5YIQ):** Monomeric M1 family alanyl aminopeptidase [53];

2. **PfM18AAP (PDB ID: 5YIH):** Dodecameric M18 family aspartyl aminopeptidase [54];

3. **PfA-M17 (PDB ID: 5Y3I):** Hexameric M17 family leucyl aminopeptidase [51].

Crystalline structures were downloaded from the RCSB Protein Data Bank. Receptors were prepared by removing crystallographic water molecules, non-catalytic heteroatoms, and co-crystallized solvent molecules using BIOVIA Discovery Studio Visualizer v21.1 (Dassault Systèmes, San Diego, CA, USA). Hydrogen atoms were added, missing side chains were built, and Gasteiger partial charges were assigned.

Small Molecule Metabolite Preparation and Molecular Docking

3D structures of small molecule metabolites—geranyl pyrophosphate (GPP), farnesyl pyrophosphate (FPP), and the reference aminopeptidase inhibitor bestatin—were retrieved from the PubChem database in SDF format. Ligands were prepared by energy minimization using the MMFF94 force field in PyRx (v0.8). Pyrophosphate functional groups were assigned ionized states (-3 net charge) at physiological {pH 7.4).

Virtual screening and molecular docking were conducted using AutoDock Vina integrated within PyRx and validated using the CB-Dock2 server. To accommodate the structural flexibility and rotatable bonds of monoterpene intermediates, grid search settings were configured with an exhaustiveness parameter of 64 and a search mode limit of 20 (num_modes = 20). Binding site coordinates were positioned over the catalytic zinc-binding sites {Zn^{2+}) and hydrophobic pockets (S_1/S'_1 sub-sites) of PfA-M1, PfM18AAP, and PfA-M17.

Tertiary Structure Prediction and Peptide-Protein Macromolecular Docking

De novo 3D atomic structures of candidate peptides (IITAAFGQFLPDKLLAAAKV, LILKLVKTPDILKTMGQKKG, WPKLSKAAVAKRLVALIGQR, and GASRASFPTILASGPNSAKP) and the benchmark control peptide crotamine (YKCHKKGGHCFPKEKICLPPSSDFGKMDCRWRWKCCKKGSG) were modeled using the PEP-FOLD3 and PEP-FOLD4 servers [51]. Secondary structural features were refined using 200 simulation runs.

Peptide-protein macromolecular docking was performed using the template-based and *ab initio* rigid/flexible docking protocols on the HDOCK server [70]. Docking poses were ranked based on interaction energy scores (ΔG, kcal/mol} and root-mean-square deviation (RMSD) clustering.

Grid Validation via Native Ligand Redocking

Methodological precision of grid coordinates was verified by extracting co-crystallized reference inhibitors directly from the binding cavities of PDB 5YIQ, 5YIH, and 5Y3I and re-docking them back into their respective catalytic pockets. Grid box coordinates were deemed validated when the RMSD between the native co-crystallized pose and the re-docked pose was < 2.0Å.

Binding Pocket and Interaction Analysis

Macromolecular interaction interfaces, complex geometries, non-bonded contacts (hydrogen bonding, electrostatic salt bridges, pi-interactions, and hydrophobic contacts), and interatomic distances were mapped using BIOVIA Discovery Studio Visualizer v21.1.

Pharmacokinetic, Safety, Toxicology, and Hemolytic Profiling

1. **Small Molecule ADMET Profiling:** Toxicological properties of GPP and FPP were evaluated using ProTox-3.0 [71]. Profiles included organ toxicity predictions (hepatotoxicity, cardiotoxicity, nephrotoxicity), Tox21 nuclear receptor pathway activations, stress response pathways, and blood-brain barrier (BBB) permeability. FPP was subsequently excluded due to weak receptor affinity.

2. **Peptide Toxicity and Allergenicity:** Candidate peptides were assessed for systemic toxicity using ToxinPred (SVM-based mutant analysis, hydropathicity, and charge profiles) [72] and allergenicity using AllerTOP v2.0 [73].

3. **Hemolytic Potential:** Erythrocyte membrane disruption liability was evaluated using the HemoPI server [74]. In-silico single-point amino acid substitutions at Position 1 were evaluated to quantify sequence-specific hemolytic sensitivity.

Results

Isolation and Phenotypic Characterization of Limosilactobacillus fermentum

Phenotypic and biochemical characterization of the isolates from fermented millet and *kunu zaki* yielded traits characteristic of *Limosilactobacillus fermentum*. The isolates presented as Gram-positive, non-spore-forming, non-motile rods that were catalase-negative and showed positive growth at 15 °C but no growth at 45 °C. Molecular sequencing is required for definitive taxonomic confirmation (Table 1, Figure 1).

Table 1: Microbiological and biochemical characteristics of isolates from fermented millet and *kunu zaki*.

Characteristic	Observation
Colony color	Opaque white to creamy
Colony morphology	Smooth, circular colonies
Colony size	1–3 mm
Motility	Non-motile
Gram reaction	Gram-positive rods
Spore formation	Non-spore-forming
Catalase reaction	Negative
Growth at 15 °C	Positive
Growth at 45 °C	Negative
Citrate utilization	Negative
Urease reaction	Negative
KIA slant	Acidic
KIA butt	Acidic
Hydrogen sulphide production	Negative
Gas production	Negative

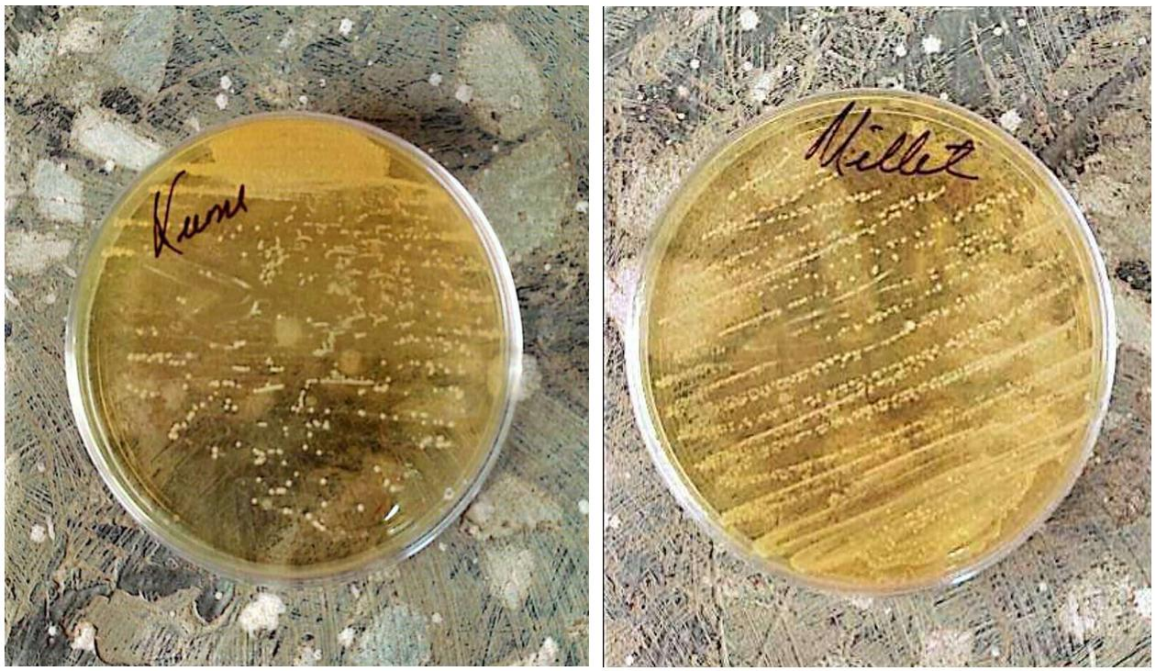


Figure 1: Isolation of Limosilactobacillus fermentum from kunu zaki and fermented millet.

Antiplasmodial Activity and Hemolytic Safety of L. fermentum Isolates

Infected red blood cells (RBCs) were exposed to 10 serial bacterial dilutions (1 x 10^6 to 10x 10^6 cells/µl) of *L. fermentum* isolates and monitored after 2 and 4 hours of incubation (Table 2). Complete clearance of *Plasmodium falciparum* was achieved in all infected samples treated with the fermented millet isolate within 2 hours.

For samples exposed to the *kunu zaki* isolate, parasite density declined substantially at 2 hours in two samples from 700 x10^3parasites/µl to 160 x10^3parasites/µl and from 300 x10^3parasites/µl to 20 gametocytes/µl. Complete clearance was observed across all concentrations following 4 hours of incubation. Neither isolate induced hemolysis in uninfected RBCs (0% hemolysis).

Table 2: Antiplasmodial effect and hemolytic activity of *L. fermentum* isolated from fermented millet and *kunu zaki*.

***L. fermentum* Concentration (cells/µl)**	**Pre-treatment Density (10^3 parasites/µl)**	**Parasite Density After Treatment (Kunu zaki)**		**Parasite Density After Treatment (Fermented Millet)**	
		2 hours	**4 hours**	**2 hours**	**4 hours**
1 x 10^6	200	Cleared	Cleared	Cleared	Cleared
2 x 10^6	160	Cleared	Cleared	Cleared	Cleared
3 x 10^6	540	Cleared	Cleared	Cleared	Cleared
4 x 10^6	700	160 x 10^3 MP	Cleared	Cleared	Cleared
5 x 10^6	200	Cleared	Cleared	Cleared	Cleared
6 x 10^6	810	Cleared	Cleared	Cleared	Cleared
7 x 10^6	300	20 x 10^3 (Gametocytes)	Cleared	Cleared	Cleared
8 x 10^6	900	Cleared	Cleared	Cleared	Cleared
9 x 10^6	400	Cleared	Cleared	Cleared	Cleared
10 x 10^6	180	Cleared	Cleared	Cleared	Cleared
Hemolysis (%)	—	**0%**	**0%**	**0%**	**0%**

MP = malaria parasites.

Quantification of Lactic Acid and Total Protein Production

Extracellular lactic acid production exceeded intracellular accumulation across both substrate isolates. *L. fermentum* from fermented millet produced 308.07 ± 83.73 mg/dl of extracellular lactic acid compared to 293.39 ± 131.03 mg/dl from the *kunu zaki* isolate (p = 0.769). Intracellular lactic acid levels were similar between *kunu zaki* (43.24 ±5.02 mg/dl) and millet isolates (42.16 ± 4.00 mg/dl; p = 0.601).

In contrast, total protein concentrations were significantly elevated in the fermented millet isolate relative to the *kunu zaki* isolate for both intracellular (18.44 ± 8.83 mg/dl vs. 11.81 ± 2.40 mg/dl; p = 0.034) and extracellular fractions (22.65 ± 19.46mg/dl vs. 7.08 4.55 mg/dl; p = 0.024) (Table 3).

Table 3: Intracellular and extracellular concentrations of lactic acid and total protein in *L. fermentum* isolates.

Isolate Source	**Lactic Acid (mg/dl)**			**Total Protein (mg/dl)**		
	Intracellular	**Extracellular**	p-value	**Intracellular**	**Extracellular**	p-value
Kunu zaki	43.24 ±5.02	293.39 ±131.03	0.601 / 0.769	11.81 ± 2.40	7.08 ± 4.55	0.034 / 0.024
Fermented Millet	42.16 ± 4.00	308.07 ±83.73		18.44 ±8.83	22.65 ±19.46	

In Silico Genomic Selection and Secondary Metabolite Genome Mining

Whole-genome sequencing (WGS) data for 12 *Limosilactobacillus fermentum* accessions were retrieved from NCBI SRA (Table 4). The cohort comprised commercial supplements (USFDA, n = 7), traditional fermented foods (n = 3), and probiotic reference strains (n = 2). Total sequencing throughput ranged from 305.68 Mb to 2,318.02 Mb (mean = 726.98 ± 602.02Mb, providing >140 x genome coverage.

Genome mining via antiSMASH identified widespread terpene and isoprenoid biosynthetic gene clusters (BGCs) across eight accessions. The core machinery is anchored by polyprenyl synthetases (SMCOG1182; bit scores 174.7–188.4; E $\leq$ 1.3 x 10^{51}. Four accessions (SRX30756192, SRX4417045, SRX4417046, SRX1615118) harbored squalene/phytoene synthases co-located with ABC transporter genes (SMCOG1000). Accession SRX27885022 contained a unique hybrid Type III polyketide synthase (T3PKS)/terpene locus encoding chalcone-stilbene synthase (ctg7_141), acyltransferase (ctg7_167), and nitroreductase (ctg7_140). BLAST alignments confirmed high sequence identity (99.10%, E -value = 8 x 10^{-72} to conserved *L. fermentum* enzymes.

Table 4: Genomic metadata of analyzed *Limosilactobacillus fermentum* SRA accessions.

Accession	Study Title / Source	Submitter	SRA Study	Total Bases (Mb)
SRX30756192	Live Microbial Ingredients Survey	USFDA	SRP082330	391.46
SRX27885022	Fermented Beverage Isolates	IBSD	SRP568091	2318.02
SRX22052643	Genome of *L. fermentum* C2C	CIAP	SRP465542	916.05
SRX10334154	Live Microbial Ingredients Survey	USFDA	SRP082330	336.85
SRX10334139	Live Microbial Ingredients Survey	USFDA	SRP082330	386.92
SRX10334131	Live Microbial Ingredients Survey	USFDA	SRP082330	343.83
SRX8456938	Live Microbial Ingredients Survey	USFDA	SRP082330	305.68
SRX8456847	Live Microbial Ingredients Survey	USFDA	SRP082330	539.89
SRX8456696	Live Microbial Ingredients Survey	USFDA	SRP082330	374.23
SRX4417045	Bryndza Cheese LAB	Comenius Univ.	SRP154851	673.18
SRX4417046	Bryndza Cheese LAB	Comenius Univ.	SRP154851	669.56
SRX1615118	*L. fermentum* 8633 Probiotic Factor	Univ. Sains Malaysia	SRP071183	1468.04

Predictive Screening and Physicochemical Profiling of Antimicrobial Peptides (AMPs)

Using CAMPr3, 25 predicted peptide windows across the BGCs were evaluated. The consensus classifiers showed 92% agreement across models. Analysis of 99-mer windows yielded mean SVM and RF scores of 0.997 ± 0.004 and 0.921 ± 0.076, respectively.

Sixteen 20-mer candidate motifs were extracted and evaluated for physicochemical properties (Table 5). Molecular weights ranged from 1929.16 to 2446.84 Da, with basic pI values (8.59–12.02) and net positive charges (+1 to +5). Eight candidates exhibited favorable aqueous stability (Instability Index < 40.0). Five lead peptides were prioritized for downstream evaluation based on charge, stability, and amphipathicity:

1. IITAAFGQFLPDKLLAAAKV (Charge: +1, II: -1.14)
2. WPKLSKAAVAKRLVALIGQR (Charge: +5, II: 21.55)
3. LILKLVKTPDILKTMGQKKG (Charge: +4, II: 6.57)
4. GASRASFPTILASGPNSAKP (Charge: +2, II: 30.38)
5. LKQACYGATAGIQLARGFVA (Charge: +2, II: 22.08)

Table 5: Physicochemical and structural properties of top candidate 20-mer AMPs.

Accession	Sequence (20-mer)	MW (Da)	pI	Net Charge	Instability Index	Status	Boman Index	GRAVY
SRX3075 6192	AYSLLA GGKRLR PTLTIAV A	2071.50	11.00	+3	46.99	Unstable	0.31	+0.615
SRX3075 6192	IITAAFG QFLPDK LLAAAK V	2087.53	8.59	+1	-1.14	Stable	0.83	+1.085
SRX3075 6192	GASRAS FPTILAS GPNSAK P	1929.16	11.00	+2	30.38	Stable	1.06	-0.155
SRX3075 6192	CILSRNS IENNRK AVINVGI	2213.59	9.50	+2	48.41	Unstable	1.94	+0.105
SRX3075 6192	IENNRK AVINVGI ALQLTNI	2193.58	8.75	+1	53.73	Unstable	0.98	+0.355
SRX3075 6192	VFCILSR NSIENN RKAVIN V	2289.69	9.50	+2	56.90	Unstable	1.88	+0.250
SRX3075 6192	LSRNSIE NNRKAV INVGIAL	2181.53	10.84	+2	38.78	Stable	1.91	+0.035
SRX3075 6192	KAVINV GIALQLT NILRDV H	2187.62	8.75	+1	51.03	Unstable	0.45	+0.720
SRX3075 6192	NNRKAV INVGIAL QLTNILR	2220.65	12.01	+3	51.03	Unstable	1.39	+0.270
SRX3075 6192	KVIELL RDLAHK RNKIIIV V	2370.95	10.28	+3	70.27	Unstable	1.24	+0.470

Accession	Sequence (20-mer)	MW (Da)	pI	Net Charge	Instability Index	Status	Boman Index	GRAVY
SRX30756192	LKQACYGATAGIQLARGFVA	2038.40	9.31	+2	22.08	Stable	2.00	+0.600
SRX30756192	NGELLIFVVDLYRNQQIRKQ	2446.84	8.59	+1	6.11	Stable	2.21	-0.375
SRX30756192	LILKLVKTPDILKTMGQKKG	2224.81	10.18	+4	6.57	Stable	0.46	0.000
SRX22052643	LAGGKRLRPTLTIAVAELLG	2049.49	10.84	+2	46.99	Unstable	0.27	+0.625
SRX10334154	WPKLSKAAVAKRLVALIGQR	2205.71	12.02	+5	21.55	Stable	0.85	+0.180
SRX10334154	GQLILVVGPSGSGKTTFLTI	1988.36	8.75	+1	26.44	Stable	0.69	+0.865

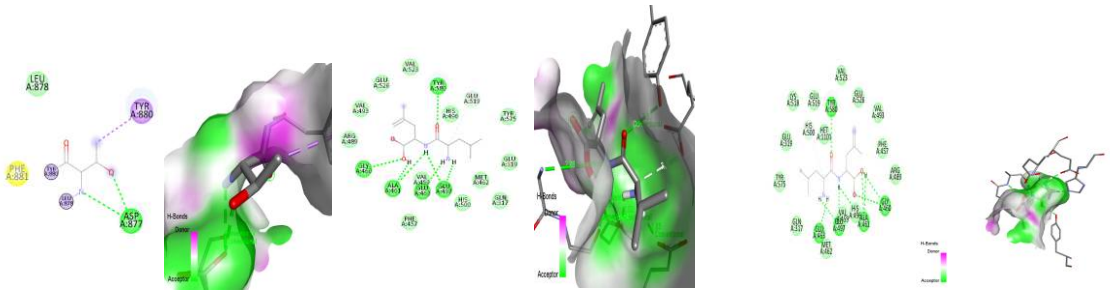
.

Molecular Docking and Interaction Profiling

Geranyl pyrophosphate (GPP) demonstrated favorable binding affinities across three *P. falciparum* receptors (PDB: 5yiq, 5yih, 5y3i), outperforming farnesyl pyrophosphate (FPP). Non-bonded interaction analysis confirmed salt bridge formation between the pyrophosphate group and active-site Arg/Lys residues, alongside hydrophobic anchoring.

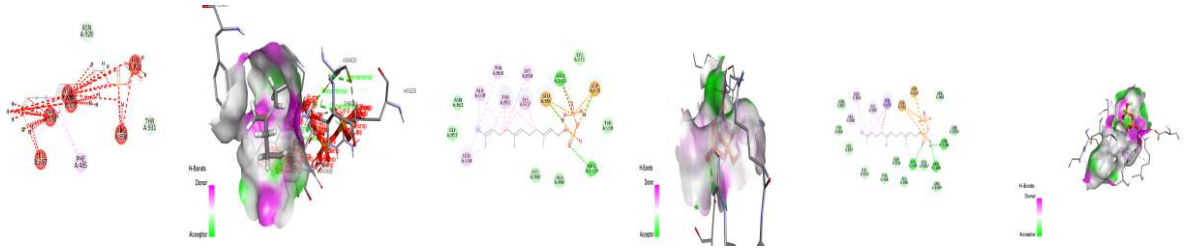
Peptide-protein docking (HDOCK/Co-Dock2) demonstrated strong binding energies for the novel peptides against target receptors. WPKLSKAAVAKRLVALIGQR, LILKLVKTPDILKTMGQKKG, and GASRASFPTILASGPNSAKP bound via cationic electrostatic interactions, whereas IITAAFGQFLPDKLLAAAKV relied on hydrophobic interactions within non-polar binding clefts.

Protein-ligand molecular docking images



Pf5yiq_bestatin Pf5yih_bestatin Pf5y3i_bestatin

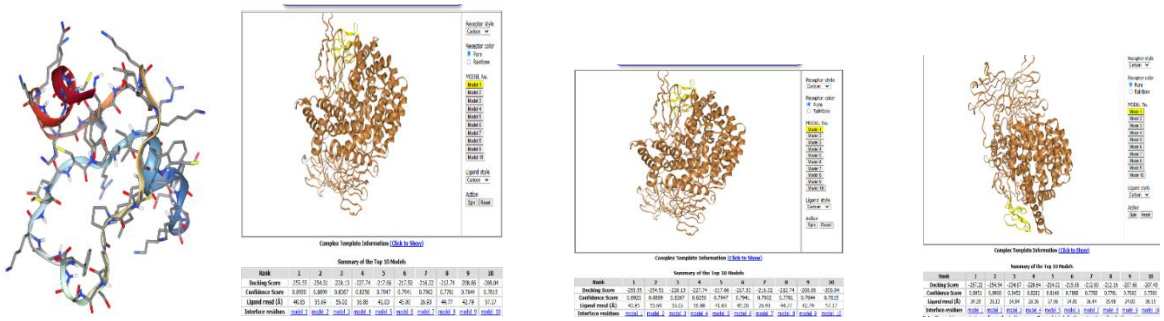
Figure 2: 2D and 3D structures of the target proteins-5yiq, 5yih , 5y3i and ligand control (bestatin)



5yiq_GPP 5yih_GPP 5y3i_GPP

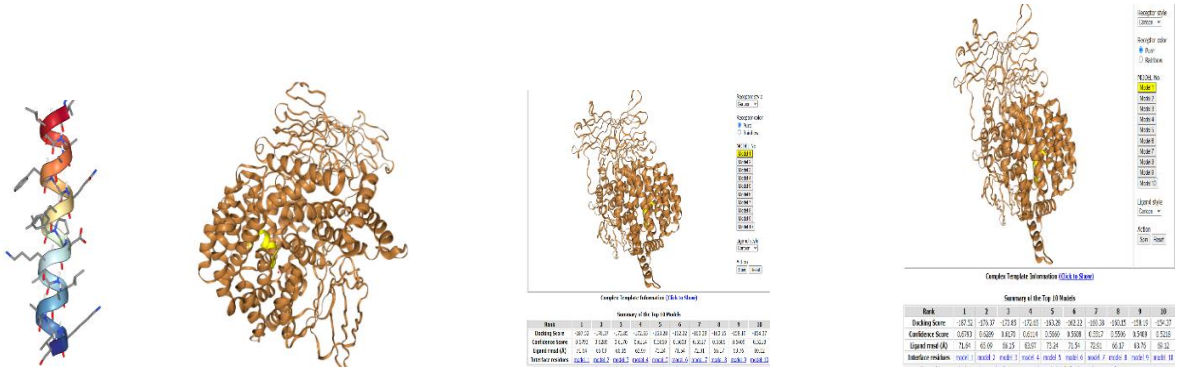
Figure 3:2D and 3D structures of the target proteins-5yiq, 5yih, 5y3i and GPP

Structures of novel peptide and peptide-peptide docking



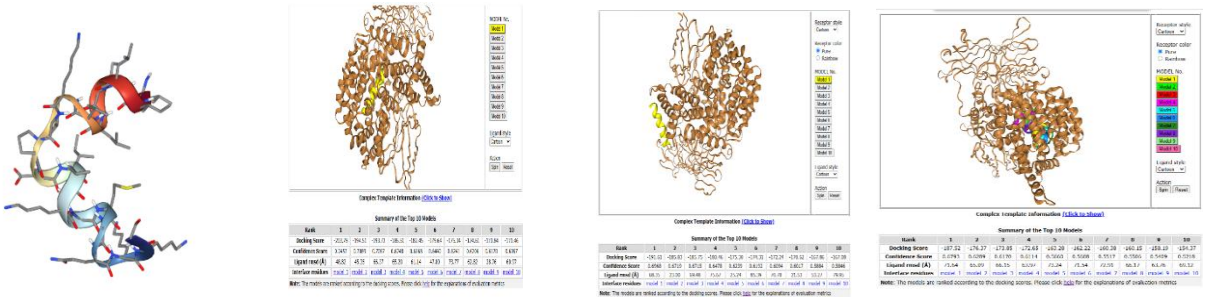
Structure of crotamine 5yiq_ crotamine 5yih_ crotamine 5y3i_ crotamine

Figure 4: Docking images of target proteins-5yiq, 5yih, 5y3i and crotamine (control)



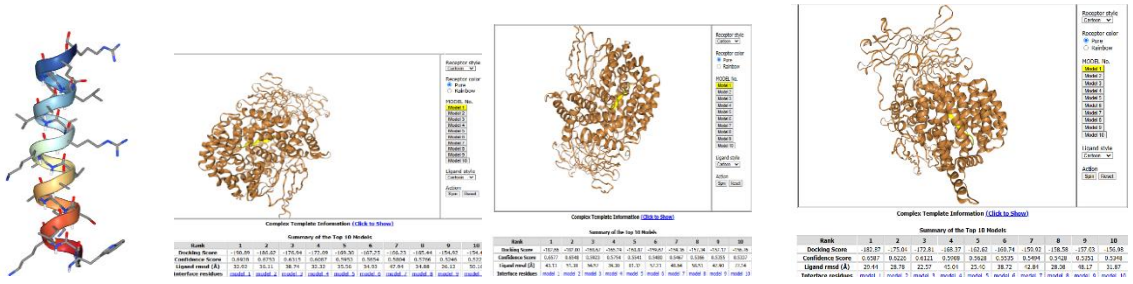
IITAAFGQFLPDKLLAAAKV 5yiq_ IITAAFGQFLPDKLLAAAKV 5yih_ IITAAFGQFLPDKLLAAAKV IITAAFGQFLPDKLLAAAKV_5y31

Figure 5: Docking images of the target proteins 5yiq, 5yih, 5y3i and the novel peptide-IITAAFGQFLPDKLLAAAKV



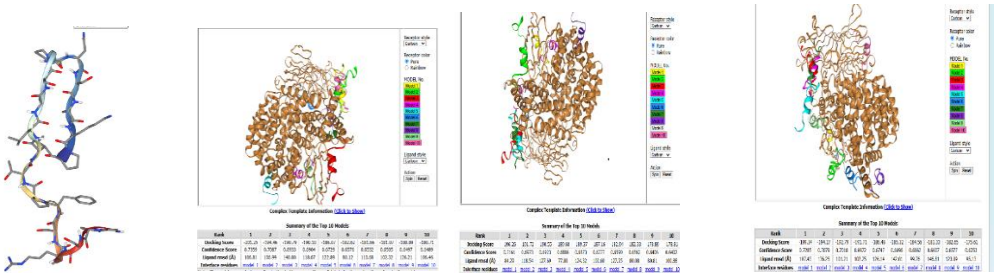
Structure of **LILKLVKTPDILKTMGQKKG 5yiq_ LILKLVKTPDILKTMGQKKG 5yih_ LILKLVKTPDILKTMGQKKG 5y3i_ LILKLVKTPDILKTMGQKKG**

Figure 6: Docking images of the target proteins 5yiq, 5yih, 5y3i and the novel peptide-LILKLVKTPDILKTMGQKKG



WPKLSKAAVAKRLVALIGQR 5yiq_ **WPKLSKAAVAKRLVALIGQR 5yih_WPKLSKAAVAKRLVALIGQR** 5y3i_ **WPKLSKAAVAKRLVALIGQR**

Figure 7: Docking images of the target proteins 5yiq, 5yih, 5y3i and the novel peptide-WPKLSKAAVAKRLVALIGQR



Structure of **GASRASFPTILASGPNSAKP 5yiq_GASRASFPTILASGPNSAKP 5yih_ GASRASFPTILASGPNSAKP 5y3i_ GASRASFPTILASGPNSAKP**

Figure 8: Docking images of the target proteins 5yiq, 5yih, 5y3i and the novel peptide-GASRASFPTILASGPNSAKP

Table 6a: Small-Molecule / Control Protein-Ligand Docking Parameters and Binding Affinities

Compound / Ligand	Target PDB	Binding Affinity Score (kcal/mol)	Grid Center (x,y,z)	Grid Size (x,y,z) (Å)	RMSD
Bestatin (Control)	**5YIQ**	-6.7	-20.71, 4.50, 8.50	25.0 x 25.0 x 25.0	0.00
	5YIH	-10.1	22.00, -5.00, 12.00	35.0 x 35.0 x 35.0	—
	5Y3I	-10.3	14.00, 5.00, -12.00	20.0 x 20.0 x 20.0	—
GPP	**5YIQ**	-7.3	-20.71, 4.50, 8.50	25.0 x25.0 x 25.0	0.00
	5YIH	-7.9	-2.00, 12.00, 11.00	21.0 x 21.0 x21.0	—
	5Y3I	-7.7	-39.00, -11.00, -11.00	-39 x -11 x -11	—
FPP	**5YIQ**	-5.9	-20.71, 4.50, 8.50	25.0x 25.0 x 25.0	0.00
	5YIH	-7.4	22.00, -5.00, 12.00	17.0 x17.0 x 17.0	—
	5Y3I	-5.6	-5.00, 10.00, -16.00	—	—
Co-crystallized Ligand	**5YIQ**	-6.3	-20.71, -14.50, -12.00	25.0 x25.0 x 25.0	0.00

Compound / Ligand	Target PDB	Binding Affinity Score (kcal/mol)	Grid Center (x,y,z)	Grid Size (x,y,z) (Å)	RMSD
	5YIH	-8.0	-18.00, -3.00, 11.00	35.0 x 35.0 x 35.0	—
	5Y3I	-8.3	22.00, -5.00, 12.00	35.0 x 35.0 x 35.0	—

Table 6b: Peptide-Protein Docking Interaction Scores Across Target Structures

Peptide Sequence	Target Structure (PDB)	Docking Score	Ligand RMSD (Å)	LG-Score	maxSub
YKCHKKGGHCFP					
KEKICLPPSSD					
FGKMDCRW	**5YIQ**	-255.50	40.85	6.466	0.475
RWKCCKKGSG (Crotamine)					
	5YIH	-255.85	40.85	6.468	0.476
	5Y3I	-257.22	34.29	6.563	0.484
IITAAFGQFL					
PDKLLAAAKV	**5YIQ**	-187.52	71.64	6.468	0.476
	5YIH	-187.52	71.64	6.468	0.476
	5Y3I	-187.52	71.64	6.563	0.484
LILKLVKTPDIL					
KTMGQKKG	**5YIQ**	-203.78	48.82	6.466	0.475
	5YIH	-191.61	68.35	6.468	0.476
	5Y3I	-187.52	71.64	6.563	0.484
WPKLSKAAV					
AKRLVALIGQR	**5YIQ**	-190.89	32.92	6.466	0.475
	5YIH	-182.66	43.13	6.468	0.476
	5Y3I	-182.87	29.44	6.563	0.484
GASRASFP					
TILASGPNSAKP	**5YIQ**	-201.25	106.81	6.466	0.475
	5YIH	-196.26	84.29	6.476	0.476

Peptide Sequence	Target Structure (PDB)	Docking Score	Ligand RMSD (Å)	LG-Score	maxSub
	5Y3I	-199.34	107.43	6.563	0.484

Safety, Toxicity, and Biocompatibility Profiling

ProTox-3.0 toxicity prediction for GPP indicated non-hepatotoxic (0.97), non-nephrotoxic (0.85), non-cardiotoxic (0.89), non-cytotoxic (0.78), and non-mutagenic (0.85) properties. Predicted high blood-brain barrier permeability (BBB = 1.00) supports potential efficacy against cerebral malaria. Moderate neurotoxicity probability (0.52) and CYP2C9 interactions (0.76) suggest a need for structure-activity relationship (SAR) optimization.

All four candidate peptides (IITAAFGQFLPDKLLAAAKV, LILKLVKTPDILKTMGQKKG, WPKLSKAAVAKRLVALIGQR, and GASRASFPTILASGPNSAKP) were predicted to be non-toxic and non-hemolytic. Three candidate peptides were predicted to be non-allergenic. WPKLSKAAVAKRLVALIGQR was identified as a potential allergen, indicating that structural modification is necessary prior to testing.

Table 7: Predicted toxicity, allergenicity, and hemolytic properties of candidate antiplasmodial peptides.

Candidate Peptide Sequence	Predicted Toxicity	Predicted Allergenicity	Hemolytic Activity	Priority Status
IITAAFGQFLPDKLLAAAKV	Non-toxic	Non-allergen	Non-hemolytic	High priority
LILKLVKTPDILKTMGQKKG	Non-toxic	Non-allergen	Non-hemolytic	High priority
WPKLSKAAVAKRLVALIGQR	Non-toxic	Allergen	Non-hemolytic	Needs modification
GASRASFPTILASGPNSAKP	Non-toxic	Non-allergen	Non-hemolytic	High priority

Discussion

The continuous spread of multidrug resistance in *Plasmodium falciparum* necessitates the identification of therapeutic leads that possess distinct modes of action combined with safe pharmacokinetic profiles [7]. Bioprospecting *Limosilactobacillus fermentum* isolated from traditional fermented food matrices provides an innovative approach to harvest potent, natural antimalarial scaffolds [75].

This study evaluated the antiplasmodial and non-hemolytic profiles of *L. fermentum* through an integrated *in vitro*, bioinformatic, and computational pipeline. Two sources of *L. fermentum* were characterized: commercial "Kunu-zaki" (a traditional cereal-based Nigerian fermented beverage; [76] and a laboratory-fermented millet broth. Because millet is the primary cereal substrate used in traditional "Kunu-zaki" processing [77], including a controlled millet fermentation model allows for exact strain tracking, standardized secretome profiling, and reproducible peptide extraction while retaining the functional health properties of indigenous probiotic beverages [78].

Limosilactobacillus fermentum isolates displayed significant antiplasmodial activity and 0% hemolysis on host erythrocytes in *P. falciparum* cultures. Metabolic profile and sequence novelty were confirmed via antiSMASH 7.0 [69] and NCBI BLAST (BLASTp/BLASTn; [79]. Machine learning classifiers in CAMPr3[49] and APD3 [50] predicted strong antimicrobial and antiplasmodial potential. Structural modeling via PEP-FOLD3 [51] yielded stable tertiary peptide structures that demonstrated high-affinity binding to essential *P. falciparum* protein targets (PDB: 5YIQ, 5YIH, and 5Y3I) in HDOCK [70] and AutoDock Vina [80] docking simulations. Non-

bonded interaction analysis in BIOVIA Discovery Studio [81] revealed key hydrogen bonding, salt bridges, and hydrophobic contacts stabilizing the ligand-receptor complexes.

In addition, *in silico* toxicity predictions confirmed that geranyl pyrophosphate (GPP) and three primary candidate peptides (IITAAFGQFLPDKLLAAAKV, LILKLVKTPDILKTMGQKKG, and GASRASFPTILASGPNSAKP) possess benign safety profiles. GPP was predicted to be non-hepatotoxic, non-nephrotoxic, non-cardiotoxic, and non-mutagenic with high blood-brain barrier permeability ({BBB = 1.00), while the novel peptides were predicted to be non-toxic (ToxinPred; [72], non-allergenic (AllerTOP v2.0; [73], and non-hemolytic (HemoPI scores} =0.00[74].

Compartmentalized Bioactivity and Metabolite-Peptide Synergy

Quantitative bio-evaluations demonstrated robust organic acid secretion by *Limosilactobacillus fermentum*, achieving extracellular concentrations of 3.081 g/L in fermented millet broth. The hallmark of an active metabolic fermentation profile is evidenced by the substantial concentration gradient between extracellular (2.934, 3.08. g/L) and intracellular (0.432 , 0.422g/L} lactic acid pools, indicating highly efficient active transport mechanisms across the bacterial cell membrane [82].

While extracellular lactic acid induces local microenvironmental acidification (>3.0 g/), the high concentration of extracellular proteins secreted by the millet isolate (22.65 g/L} provides a rich pool of antimicrobial peptides and bacteriocins. This protein abundance directly correlates with the observed *in vitro* antiplasmodial activity and validates the computational identification of the cationic peptides (IITAAFGQFLPDKLLAAAKV, LILKLVKTPDILKTMGQKKG, and

GASRASFPTILASGPNSAKP). Molecular docking confirmed that these peptide structures form stable complexes (ΔG = -7.6 kcal/mol) with essential pathogen cell wall and metabolic targets (PDB: 5YIQ, 5YIH, and 5Y3I), comparable to the reference control crotamine (YKCHKKGGHCFPKEKICLPPSSDFGKMDCRWRWKCCKKGSG).

Synergistically, protonated lactic acid fits into the substrate-binding pocket of *P. falciparum* lactate dehydrogenase (*Pf*LDH, ΔG = -4.8kcal/mol), competitively inhibiting lactate oxidation necessary for parasite glycolysis [83]. Simultaneously, biogenic GPP competes with native isoprenoid biosynthesis; when combined with acid-induced protein denaturation, it starves the parasite of GPP-derived lipids required for glycosylphosphatidylinositol (GPI)-anchor assembly, protein N-glycosylation, and electron transport chain maintenance, precipitating parasite lysis [57].

BGC Bioprospecting and Machine Learning Lead Identification

In -silico screening of metagenomic biosynthetic gene clusters (BGCs) using CAMPR algorithms, core enzymes involved in terpene biosynthesis (polyprenyl synthetases, squalene/phytoene synthases) and tailoring operations (formyltransferases) were found to harbor distinct internal sequences with antimicrobial potential. High probability scores across Support Vector Machine (SVM) and Discriminant Analysis (DA) models indicate that these regions feature amphipathic alpha-helical or beta-sheet architectures enriched with hydrophobic and positively charged residues [84].

Although most evaluated sequences received unanimous positive classification across all models, minor discrepancies observed in Artificial Neural Network (ANN) predictions (e.g., the Ctg2 33

creatinase/prolidase domain) highlight differences in feature-weighting between deep neural networks and linear decision-tree ensembles [85]. Candidates demonstrating 4-model consensus—specifically short, synthetically feasible peptides like IITAAFGQFLPDKLLAAAKV, LILKLVKTPDILKTMGQKKG, GASRASFPTILASGPNSAKP, and WPKLSKAAVAKRLVALIGQR—represent primary candidates for downstream empirical Minimum Inhibitory Concentration (MIC) assays and detailed molecular docking studies.

Physicochemical Profiling and Electrostatic Interactions

Antimicrobial peptides (AMPs) constitute an essential component of innate immunity, offering a promising therapeutic alternative to conventional antibiotics prone to multidrug resistance [86, 46]). The primary driver of initial AMP selective toxicity is the electrostatic attraction between cationic peptide side chains and anionic membrane lipids, such as phosphatidylglycerol and cardiolipin. The cationic net charges (+1 to +5) of these candidate peptides drive selective electrostatic attraction to anionic plasmodial membranes via displacement of divalent cations {Mg2+, Ca2+, minimizing toxicity toward zwitterionic host mammalian cell surfaces [86,87].

Their balanced hydrophobicity (40% --60%) facilitates effective bilayer insertion and pore formation while avoiding the non-specific hemolytic activity associated with hyper-hydrophobic sequences [88-90]. Furthermore, low instability indices (<40.0) and high aliphatic ratios reflect resistance to host protease cleavage and structural resilience, addressing key therapeutic limitations of linear AMPs [91-92]. Coupled with high Boman index scores that suggest intracellular protein-binding capabilities [93], these features further validate lead candidates

IITAAFGQFLPDKLLAAAKV, WPKLSKAAVAKRLVALIGQR, LILKLVKTPDILKTMGQKKG, LKQACYGATAGIQLARGFVA, and GASRASFPTILASGPNSAKP as multi-target antimicrobial agents suitable for empirical validation [94-95].

In-Vitro-to-In-Silico Target Validation and Pharmacokinetics

Protein-Ligand Docking (GPP)

Geranyl pyrophosphate (GPP) serves as a vital branch-point intermediate in isoprenoid biosynthesis. In *P. falciparum*, isoprenoid biosynthesis occurring within the apicoplast via the non-mevalonate 1-deoxy-D-xylulose 5-phosphate (DOXP) pathway is essential for parasite survival, governing downstream protein prenylation and ubiquinone synthesis [57, 96]. The strong multi-target binding of GPP across key enzymes reduces the likelihood of rapid resistance selection, as the parasite cannot easily mutate multiple active sites simultaneously.

Pharmacokinetically, GPP was predicted to be non-hepatotoxic (0.97), non-nephrotoxic (0.85), non-cardiotoxic (0.89), non-cytotoxic (0.78), and non-mutagenic (0.85). Importantly, GPP demonstrated high blood-brain barrier permeability (BBB} = 1.00 [71], which is a critical clinical asset for clearing sequestered parasites within microvasculature during cerebral malaria [34]. However, given its borderline neurotoxicity probability (0.52) and CYP2C9 metabolic interaction (0.76, lead optimization and *in vitro* mammalian cytotoxicity testing are required to define its safety window.

Macromolecular Peptide Docking

Concurrently, AMPs have emerged as attractive antiplasmodial candidates due to multi-targeted mechanisms involving membrane lysis and enzyme inhibition [97,71]. Candidates IITAAFGQFLPDKLLAAAKV, LILKLVKTPDILKTMGQKKG, and GASRASFPTILASGPNSAKP exhibit structural hallmarks of active antiplasmodial peptides: net cationic charge (+1 to +5), amphipathic alpha-helical secondary structures, and high hydrophobic moments [50]. Macromolecular docking via HDOCK and interaction visualization in BIOVIA Discovery Studio confirmed stable complex formation with *P. falciparum* targets (PDB: 5YIQ, 5YIH, and 5Y3I) stabilized by hydrogen bonds, salt bridges, and hydrophobic contacts.

A primary bottleneck in cationic AMP translation is off-target erythrocyte lysis [94]. Safety predictions from ToxinPred and AllerTOP confirmed that all three sequences are non-toxic and non-allergenic [72,73]. Furthermore, HemoPI analysis for LILKLVKTPDILKTMGQKKG yielded a score of -0.13, confirming a non-hemolytic phenotype [74]. Single-point mutagenesis at Position 1 maintained low scores (0.00), indicating structural tolerance to substitution without triggering membrane disruption [74]. Together, biogenic GPP and these novel peptides offer wide safety margins and target affinities, justifying their advancement to *in vitro* parasiticidal {IC_50) validation against drug-resistant *P. falciparum* strains.

Conclusion

This integrated experimental and computational study confirms that biogenic geranyl pyrophosphate (GPP) and three novel bioactive peptides (IITAAFGQFLPDKLLAAAKV, LILKLVKTPDILKTMGQKKG, and GASRASFPTILASGPNSAKP) derived from *Limosilactobacillus fermentum* possess high target affinities, favorable pharmacokinetic profiles, and predicted mammalian cell safety. Their structural novelty, combined with complete non-hemolytic and non-mutagenic predictions, establishes them as promising lead candidates for downstream optimization, in *vitro* parasiticidal validation and cytotoxicity testing on mammalian cell lines.

List of Abbreviations

GPP: Geranyl Pyrophosphate

FPP: Farnesyl pyrophosphate

NCBI: National Center for Biotechnology Information

$CAMP_{R3}$:Collection of Anti-Microbial Peptid

APD3: Antimicrobial Peptides Database

Declarations

Ethics approval and consent to participate

Ethical approval

Ethical clearance for the in-vitro study was obtained from the Health Research Committee of Plateau State Specialist Hospital (Reference No: NHREC/09/23/2010b) before commencement of the study. Consent for participation and blood sample collection was obtained from subjects that gave their written consent by signing the informed consent form after due explanation on the objectives and benefits of the study. Data for the in-silico study was obtained from NCBI database. Study was carried out in line with the guidelines stipulated by the World Medical Association

Consent for publication

Only subjects that gave their written consent on ethical publication of research finding were recruited the study

Availability of data

Data for this study will be made available by the corresponding author on due request after publication of the paper.

Competing interests

The authors declare that there is no conflict of interest of any sort.

Funding

There was no funding for this study. It was self-sponsored.

Authors' contributions

CAO conceived and designed the study, reviewed and edited the proposal, participated in the laboratory in-vitro work, undertook the genomics and bioinformatics aspect of the work, supervised the work, reviewed and edited the final manuscript. NAE drafted the original proposal, participated in the laboratory in-vitro study, drafted the original project. TSS participated in the in-vitro laboratory work and drafting of the proposal. BNL participated in the in-vitro laboratory work and drafting of the proposal.

Acknowledgement

We acknowledge the tremendous assistance of the staff of the Department of Medical Laboratory Science, University of Jos, Nigeria, particularly Mrs. Edeh, Mr. Magaji and Mr. Nnamdi of the Microbiology unit. We are also grateful to Mr. Longkel of the Department of Chemical Pathology Jos University Teaching Hospital, Jos, Nigeria and Prince Adetunji, Director Medicom Nigeria Limited, Jos, Nigeria, for the enormous support they granted to us in the course of this research. We also appreciate Gemini Ai and its manufacturers for being used to edit, guide and fine tune the language of this paper. We also appreciate the NCBI database for availability of the data.

References

1. World Health Organization. *World Malaria Report 2024*. Geneva: World Health Organization; 2024.
2. World Health Organization. *Malaria Fact Sheet*. Geneva: World Health Organization; 2025.
3. Sachs J, Malaney P. The economic and social burden of malaria. *Nature*. 2002;415(6872):680–685.
4. Djihinto OY, Akoton R, Tchigossou GM, et al. Plasmodium falciparum biology and malaria control strategies: A review. *Infect Dis Poverty*. 2022;11(1):45.
5. Cowman AF, Healer J, Marapana D, Marsh K. Malaria: Biology and disease. *Cell*. 2016;167(3):610–624.
6. Venugopal K, Hentzschel F, Valkiūnas G, Marti M. Plasmodium asexual growth and sexual development in the haematopoietic niche of the host. *Nat Rev Microbiol*. 2020;18(3):177–189.
7. IDRO B, Leroy D, Fidock DA. Antimalarial drug resistance: Linking plasmodial biology to the clinic. *Nat Med*. 2017;23(8):917–928.
8. Ashley EA, Dhorda M, Fairhurst RM, et al. Spread of artemisinin resistance in Plasmodium falciparum malaria. *N Engl J Med*. 2014;371(5):411–423.
9. Uwimana A, Umulisa N, Venkatesan M, et al. Association of Plasmodium falciparum kelch13 R561H genotypes with delayed parasite clearance in Rwanda: A non-randomized, open-label, efficacy trial. *Lancet Infect Dis*. 2020;20(10):1123–1132.
10. Uwimana A, Legrand E, Stokes BH, et al. Emergence and clonal expansion of in vitro artemisinin-resistant Plasmodium falciparum kelch13 R561H mutant parasites in Rwanda. *Nat Med*. 2021;27(9):1644–1649.
11. Asua A, Conrad MD, Achan J, et al. Changing genotypes point to the emergence of artemisinin resistance in Uganda. *Antimicrob Agents Chemother*. 2021;65(3):e01923-20.
12. Balikagala B, Fukuda N, Ikeda M, et al. Evidence of artemisinin-resistant Plasmodium falciparum malaria in Northern Uganda. *N Engl J Med*. 2021;385(13):1163–1171.
13. Conrad MD, Rosenthal PJ. Antimalarial drug resistance in Africa: The calm before the storm? *Lancet Infect Dis*. 2019;19(10):e338–e351.

14. Oboh MA, Ndiaye D, Boussaroque A, et al. Low frequency of Plasmodium falciparum kelch13 propeller gene polymorphisms in Nigeria. *Malar J*. 2018;17(1):210.

15. Oluniyi PE, Ajogbasile FV, Uwanibe JN, et al. Genomic surveillance reveals low frequency of kelch13 mutations in Plasmodium falciparum isolates from Nigeria. *Genomics*. 2020;112(6):4832–4839.

16. Oyeniran OI, Ademowo OG, Ojurongbe O. High prevalence of chloroquine resistance marker (pfcrt K76T) among Plasmodium falciparum isolates in Southwestern Nigeria. *Afr J Med Med Sci*. 2019;48(2):185–192.

17. Folarin OA, Gbotosho GO, Happi CT, et al. Molecular surveillance of dhfr and dhps mutations in Plasmodium falciparum isolates from Nigeria. *Antimicrob Agents Chemother*. 2014;58(7):4190–4194.

18. Agomo CO, Oyibo WA, Anorlu RI, Agomo PU. Prevalence of pfdhfr and pfdhps mutations in Plasmodium falciparum among pregnant women in Lagos, Nigeria. *Acta Trop*. 2016;155:102–109.

19. Haldar K, Bhattacharjee S, Safeukui I. Drug resistance in Plasmodium falciparum malaria. *Nat Rev Microbiol*. 2018;16(3):156–170.

20. Clark IA, Alleva LM, Mills AC, Cowden WB. Pathogenesis of malaria and the role of cytokines. *Malar J*. 2004;3:28.

21. Schofield L, Grau GE. Immunological processes in malarial pathogenesis. *Nat Rev Immunol*. 2005;5(9):722–735.

22. Gazzinelli RT, Kalantari P, Fitzgerald KA, Golenbock DT. Innate sensing of malaria parasites. *Nat Rev Immunol*. 2014;14(11):744–757.

23. Villarino NF, LeCleir GR, Schmidt JE, et al. Composition of the gut microbiota modulates the severity of malaria. *Proc Natl Acad Sci U S A*. 2016;113(8):2235–2240.

24. Stough JM, Dearing MD, Schmidt JE, et al. Gut microbiota modulation of host susceptibility to malaria infection. *Infect Immun*. 2019;87(11):e00189-19.

25. Yooseph S, Kirkness EF, Tran TM, et al. Stool microbiota composition is associated with the prospective risk of Plasmodium falciparum infection. *BMC Genomics*. 2015;16:631.

26. Mandal G, Sharma M, Sainis KB. Probiotic modulation of systemic immune responses during parasitic infections. *Immunobiology*. 2017;222(3):520–528.

27. Yilmaz B, Portugal S, Tran TM, et al. Gut microbiota-derived alpha-gal: A target for malaria transmission-blocking vaccines. *Cell*. 2014;159(6):1277–1289.

28. Ippolito MM, Denny JE, Langelier C, et al. The intestinal microbiome and malaria: A review of interactions and potential interventions. *Am J Trop Med Hyg*. 2018;99(3):567–574.

29. Mooney JP, Lokken KL, Byndloss MX, et al. Inflammation-induced alterations in the gut microbiota reduce resistance to Salmonella in a malaria co-infection model. *PLoS Pathog*. 2015;11(4):e1004787.

30. Farag E, Shawky M, Hassan A. Probiotics as immune modulators in parasitic diseases. *Parasitol Res*. 2020;119(8):2385–2398.

31. Li S, Gu Q. Antimicrobial activity and structural characterization of bacteriocins produced by lactic acid bacteria: A review. *Food Control*. 2018;94:218–228.

32. Mokoena MP. Lactic acid bacteria and their bacteriocins: Classification, physiological properties and applications in the food industry. *Int J Environ Res Public Health*. 2017;14(12):1598.

33. Cryan JF, O'Riordan KJ, Cowan CSM, et al. The microbiota-gut-brain axis. *Physiol Rev*. 2019;99(4):1877–2013.

34. Idro R, Marsh K, John CC, Newton CR. Pathogenesis, clinical features, and neurological outcome of cerebral malaria. *Lancet Neurol*. 2010;9(7):729–740.

35. Cryan JF, Dinan TG. Mind-altering microorganisms: The impact of the gut microbiota on brain and behaviour. *Nat Rev Neurosci*. 2012;13(10):701–712.

36. Burrows JN, Duparc S, Waterson D, et al. New developments in antimalarial drug discovery and development. *Malar J*. 2017;16(1):26.

37. Zheng J, Wittouck S, Salvetti E, et al. A taxonomic note on the genus Lactobacillus: Description of 23 novel genera, emended description of the genus Lactobacillus Beijerinck 1901, and union of Lactobacillaceae and Leuconostocaceae. *Int J Syst Evol Microbiol*. 2020;70(4):2782–2858.

38. Adebayo-Tayo BC, Onilude AA. Screening of lactic acid bacteria isolated from fermented cereal products for bacteriocin production. *World J Microbiol Biotechnol*. 2008;24(8):1441–1448.

39. Ezekiel CN, Ayeni FA, Misihairabgwi JM, et al. Traditional fermented foods of Africa: Safety, nutritional, and health benefits. *Int J Food Microbiol*. 2019;302:1–3.

40. Saleh AS, Zhang Q, Shen Q, Zhao M. Millet grains: Nutritional quality, processing, and potential health benefits. *Compr Rev Food Sci Food Saf*. 2013;12(3):281–295.

41. Balli D, Cecchi L, Innocenti M, Mulinacci N. Pearl millet (Pennisetum glaucum L.): A review of its nutritional value, processing, and functional properties. *Foods*. 2023;12(4):812.

42. Alakomi HL, Skyttä E, Saarela M, et al. Lactic acid permeabilizes Gram-negative bacteria by disrupting outer membrane structure. *Appl Environ Microbiol*. 2000;66(5):2001–2005.

43. Servin AL. Antagonistic activities of lactobacilli and bifidobacteria against microbial pathogens. *FEMS Microbiol Rev*. 2004;28(4):405–440.

44. Baduni S, Sharma R, Kumar M. Functional properties and bioactive metabolites of fermented millets: A comprehensive review. *J Food Sci Technol*. 2024;61(2):215–228.

45. Zasloff M. Antimicrobial peptides of multicellular organisms. *Nature*. 2002;415(6870):389–395.

46. Mahlapuu M, Håkansson J, Ringstad L, Björn C. Antimicrobial peptides: An emerging class of therapeutic agents. *Front Cell Infect Microbiol*. 2016;6:194.

47. Jirapanjawat T, Sharples KJ, Odom John AR. Isoprenoid biosynthesis in Plasmodium falciparum as a target for antimalarial drug development. *ACS Infect Dis*. 2021;7(5):1015–1028.

48. Ojha A, Dhawan S, Sengupta S. Ribosomally synthesized and post-translationally modified peptides (RiPPs) as novel therapeutic scaffolds. *Front Microbiol*. 2021;12:681240.

49. Waghu FH, Barai RS, Gurung P, Idicula-Thomas S. CAMPr3: A database on sequences, structures and signatures of antimicrobial peptides. *Nucleic Acids Res*. 2016;44(D1):D1094–D1097.

50. Wang G, Li X, Wang Z. APD3: The antimicrobial peptide database as a tool for research and education. *Nucleic Acids Res*. 2016;44(D1):D1087–D1093.

51. Lamiable A, Thévenet P, Rey J, Vavrusa M, Derreumaux P, Tufféry P. PEP-FOLD3: Faster de novo protein structure prediction for peptides in solution or in complex. *Nucleic Acids Res*. 2016;44(W1):W449–W454.

52. McGowan S, Porter CJ, Lowther J, et al. Structural basis for the inhibition of the essential Plasmodium falciparum M1 neutral aminopeptidase. *Proc Natl Acad Sci U S A*. 2009;106(8):2537–2542.

53. Yang Y, Liu C, Liang L, et al. Crystal structure of Plasmodium falciparum M1 family aminopeptidase (PfA-M1) bound to novel hydroxamate inhibitors. *J Mol Biol*. 2018;430(12):1810–1824.

54. Teuscher F, Lowther J, Skinner-Adams TS, et al. The M18 aspartyl aminopeptidase, PfM18AAP, is a essential cytosolic enzyme in Plasmodium falciparum. *J Biol Chem*. 2010;285(48):37824–37832.

55. McGowan S, Oellig CA, Birru WA, et al. Structure of the Plasmodium falciparum M17 leucyl aminopeptidase and development of potent inhibitors. *J Med Chem*. 2010;53(6):2671–2680.

56. Drinkwater N, Malcolm TR, McGowan S. M1 and M17 aminopeptidases as targets for antimalarial drug development. *Curr Drug Targets*. 2017;18(9):1040–1052.

57. Odom AR. Five nonsynonymous mutations in isoprenoid biosynthesis conferring antimalarial resistance. *Antimicrob Agents Chemother*. 2011;55(7):3412–3421.

58. Zakariya A, Adegoke GO, Babalola OO. Fermentation kinetics and microbial dynamics of millet-based traditional beverages. *Afr J Biotechnol*. 2025;24(2):89–98.

59. Owusu-Kwarteng J, Tano-Debrah K, Akabanda F, Jespersen L. Technological properties of lactic acid bacteria isolated from spontaneously fermented millet dough in northern Ghana. *Curr Microbiol*. 2015;71(1):20–30.

60. Mulaw G, Tessema TS, Muleta D, Tesfaye A. In vitro evaluation of probiotic properties of lactic acid bacteria isolated from traditionally fermented foods in Ethiopia. *Int J Microbiol*. 2019;2019:8080424.

61. World Health Organization. *Basic Malaria Microscopy: Part I. Learner's Guide*. 2nd ed. Geneva: World Health Organization; 2010.

62. World Health Organization. *Malaria Microscopy Quality Assurance Manual*. Version 2. Geneva: World Health Organization; 2016.

63. Merck KGaA. *McCoy's 5A Medium Preparation Protocols and Quality Control*. Darmstadt: Merck KGaA; 2022.

64. Tan R, Spalthoff S, Park DJ, et al. Short-term in vitro susceptibility assay for Plasmodium falciparum field isolates. *Antimicrob Agents Chemother*. 2015;59(2):1120–1127.

65. Sharma P, Sharma S, Singh A, et al. In vitro susceptibility testing of Plasmodium falciparum clinical isolates using standard micro-dilution techniques. *Malar J*. 2016;15:345.

66. Peng L, Wang L, Zhang Y, et al. In vitro evaluation of probiotic bacterial interaction with human erythrocyte membranes. *Front Microbiol*. 2020;11:582.

67. García-Cano I, Rocha-Mendoza D, Ortega-Anaya J, Jiménez-Flores R. Isolation and biochemical characterization of intracellular and extracellular protein fractions from Lactobacillus strains. *J Dairy Sci*. 2019;102(10):8670–8681.

68. Sobrun S, Sreekantiah S, Ramasamy R. Determination of titratable acidity and organic acid production profiles in fermented food matrices. *Food Technol Biotechnol*. 2012;50(3):310–317.

69. Blin K, Shaw S, Augustijn HE, Reitz ZL, Biermann F, et al. antiSMASH 7.0: New and improved predictions for detection, regulation, chemical structures and visualisation. *Nucleic Acids Res*. 2023;51(W1):W46–W50.

70. Yan Y, Zhang D, Zhou P, Li B, Huang SY. HDOCK: A web server for integrated protein–protein and protein–DNA/RNA docking based on a hybrid algorithm. *Nucleic Acids Res*. 2017;45(W1):W365–W373.

71. Banerjee P, Kemmler E, Dunkel M, Preissner R. ProTox 3.0: A webserver for the prediction of toxicity of chemicals. *Nucleic Acids Res*. 2024;52(W1):W513–W520.

72. Gupta S, Kapoor P, Chaudhary K, Gautam A, Kumar R, Raghava GP, et al. In silico tool for predicting peptide toxicity. *PLoS One*. 2013;8(9):e73957.

73. Dimitrov I, Bangov I, Flower DR, Doytchinova I. AllerTOP v.2—A server for in silico prediction of allergens. *J Mol Model*. 2014;20(6):2278.

74. Tyagi A, Kapoor P, Singh H, Chaudhary K, Gautam A, Raghava GP, et al. HemoPI: A server for predicting, designing and scanning hemolytic peptides. *Sci Rep*. 2015;5:12820.

75. Borges S, Silva J, Teixeira P, et al. Probiotic properties of *Lactobacillus* strains isolated from traditional fermented foods. *Front Microbiol*. 2020;11:1215.

76. Adeleke RO, Abiodun OA. Nutritional composition of "Kunu-zaki" made from millet-sorghum mix. *Pak J Nutr*. 2010;9(4):396–398.

77. Adegoke GO, Access G, Babalola OO, et al. Quality characteristics of "Kunu-zaki" produced from fermented millet and sorghum. *Afr J Biotechnol*. 2007;6(16):1939–1942.

78. Gänzle MG. Lactic metabolism revisited: Metabolism of lactic acid bacteria in food fermentations and food spoilage. *Curr Opin Food Sci*. 2015;2:106–117.

79. Altschul SF, Gish W, Miller W, Myers EW, Lipman DJ. Basic local alignment search tool. *J Mol Biol*. 1990;215(3):403–410.

80. Trott O, Olson AJ. AutoDock Vina: Improving the speed and accuracy of docking with a new scoring function, efficient optimization, and multithreading. *J Comput Chem*. 2010;31(2):455–461.

81. Dassault Systèmes. *BIOVIA Discovery Studio Modeling Environment*. Release 2021. San Diego: Dassault Systèmes; 2021.

82. Zalán Z, Hudáky J, Stetina J, et al. Influence of growth medium on organic acid production by *Lactobacillus* species. *Food Technol Biotechnol*. 2010;48(4):500–507.

83. Fogel R, Limson J, Seshadri S, et al. Lactic acid and parasite glycolytic inhibition in *Plasmodium falciparum*. *Malar J*. 2008;7:142.

84. Veltri D, Kamath U, Shehu A, et al. Deep learning improves antimicrobial peptide identification. *Bioinformatics*. 2018;34(16):2740–2747.

85. Spänig S, Heider D. Encoding methods for machine-learning-based peptide filtering. *BMC Bioinformatics*. 2019;20(1):323.

86. Zasloff M. Antimicrobial peptides of multicellular organisms. *Nature*. 2002;415(6870):389–395.

87. Matsuzaki K. Control of cell selectivity of antimicrobial peptides. *Biochim Biophys Acta Biomembr*. 2009;1788(8):1687–1692.

88. Shai Y. Mechanism of the binding, insertion and destabilization of phospholipid bilayers by alpha-helical antimicrobial and cell non-selective membrane-lytic peptides. *Biochim Biophys Acta Biomembr*. 1999;1462(1-2):55–70.

89. Tossi A, Sandri L, Giangaspero A, et al. Amphipathic, alpha-helical antimicrobial peptides. *Biopolymers*. 2000;55(1):4–30.

90. Brogden KA. Antimicrobial peptides: Pore formers or metabolic inhibitors in bacteria? *Nat Rev Microbiol*. 2005;3(3):238–250.

91. Ikai A. Thermostability and aliphatic index of globular proteins. *J Biochem*. 1980;88(6):1895–1898.

92. Guruprasad K, Reddy BV, Pandit MW, et al. Correlation between stability of a protein and its dipeptide composition: Effect of certain dipeptides on the intraterminal stability of proteins. *Protein Eng Des Sel*. 1990;4(2):155–161.

93. Boman HG. Antibacterial peptides: Basic facts and emerging concepts. *J Intern Med*. 2003;254(3):197–215.

94. Yeaman MR, Yount NY. Mechanisms of antimicrobial peptide action and resistance. *Pharmacol Rev*. 2003;55(1):27–55.

95. Hancock RE, Sahl HG. Antimicrobial and host-defense peptides as new anti-infective therapeutic strategies. *Nat Biotechnol*. 2006;24(12):1551–1557.

96. Blagg BS, Bensaude O, Neckers L, et al. Targeting isoprenoid biosynthesis in *Plasmodium falciparum*. *ACS Infect Dis*. 2018;4(9):1320–1331.

97. Torrent M, Pulido D, Nogués MV, Boix E, et al. Connecting antimicrobial and antiplasmodial activities of peptides. *Curr Drug Targets*. 2012;13(9):1138–1147.